HIGH PERFORMANCE VISIBLE LIGHT PHOTOCATALYTIC ACTIVITY OF MGO NANOSTRUCTURES BY USING SIMPLE SOL-GEL TECHNIQUE

V.T. Srisuvetha[1], S.L. Rayar[2], G. Shanthi[3]
[1]Department of Physics, Research Center Women's Christian College, Nagercoil.K.K. , Tamilnadu, South. India
[2]Department of Physics, St. Jude's College, Thoothoor, K.K., Tamilnadu, South.India
[3]Manonmaniam Sundaranar University, Abishekapatti, Tirunelveli, TamilNadu, India.

Abstract

In this report, we prepared MgO nanostructures by a novel and simple sol-gel method using magnesium nitrate and collusion as starting material. The method involves the hydrolysis of magnesium alkoxide in the presence of oxalic acid catalysts followed by a polyethylene glycol condensation reaction. Powder XRD results suggest that MgO nanoparticles belong to Face Centered Cubic (FCC) structured MgO nanopowders with space group of Fm-3m and the results are good agreement with the standard value (JCPDS file no. 89-7746). FESEM images reveals that platelets and nanorods shaped morphology is observed by using PEG and oxalic acid assisted MgO respectively. A considerable red shift in the absorption edge and decreasing the band gap was observed for PEG assisted sample than oxalic assisted MgO. The XPS results confirms that Mg in 2+ sate in the MgO nanocrystals. A large number of surface defects were observed through photoluminescence spectra analysis. The photocatalytic activity of MgO catalyst was investigated by using phenol and congo-red under visible light irradiation. The results demonstrate that the PEG assisted MgO showed high catalytic efficiency (95%) and good cyclic stability towards CR dye than phenol (90%). The possible photocatalytic mechanism also discussed in detail.

Index Terms: MgO nanostructures; sol-gel; optical properties; visible light; congo-red.

I. INTRODUCTION

Wide band-gap oxide semiconductors, when doped with transition metal ions have attracted much attention for their promising versatile applications. Heterogeneous photocatalytic decomposition of natural pollutants is a standout amongst the most encouraging process for air and water purification. Further, semiconductor vivacious heterogeneous photocatalysis utilizing different functional nanomaterials are seriously examined for the degradation of several recalcitrant compounds in the aqueous medium and gaseous phase under UV/visible light. Recently metal oxide nanomaterials scuh as TiO_2, ZnO, SnO_2 and WO_3 [1-4] are the quintessential photocatalyst, a material that enables a response to occur in the presence. Among them, magnesium oxide (MgO) has pulled in impressive consideration because of its excellent properties, for example, high melting point (~2830 ^oC), low warmth capacity, high secondary electron discharge, high catalysis action, and solid microwave absorption capacity. Significantly, MgO nanosized powders can be utilized as catalyst in chemical industries [5-8] and catalyst support for various reactions [9-11]. Furthermore, MgO ceramic has superior thermal and mechanical properties for optical applications [12,13]. Very recently, MgO nanoflakes have been used as photocatalyst for degradation of methyl orange [14].

Generally, the surface area, morphology, agglomeration state, narrow size distribution, and synthetic process of the metal oxide nanomaterials are highly important for various properties and final applications especially in the application of photocatalyst. In recent years, a numerous MgO nanostructures have been successfully prepared using different techniques. For instance, MgO with various morphologies, such as rods, flowers, house of cards, flakes, spheres, hexagonal plates, and cubes, was synthesized via hydrothermal or solvothermal method under different conditions [15]. In order to further improvement in the photocatalytic performance, this work we prepared MgO with different nanostructures such as nanoplatelets and nanorods using simple sol-gel method. Moreover, the sol gel techniques do not require any sophisticated instrument, long time process and high temperature. This method produces chemical homogeneity, uniform morphology with large surface area and high yield of the pure products. To the best of the author's knowledge, this is the first preliminary report about structural, morphological, optical and photocatalytic properties of MgO by a simple sol gel method.

II. EXPERIMENTAL PROCEDURE

2.1 Materials

Magnesium acetate tetrahydrate $Mg(CH_3COO)_2 \cdot 4H_2O$, polyethylene glycol (PEG-400), oxalic acid (C2H2O4) and ethanol (C_2H_5OH) was purchased from Sigma- Aldrich (purity 99.97%). Phenol and congo-red (CR) dyes were purchased from Merck. As all these chemicals are analytical Grade, they were used without further purification.

2.2. Preparation of MgO photocatalyst

In the typical experimental process, magnesium acetate tetrahydrate added with 150 ml ethanol stir with half an hour to make 0.1 M solution. Then added appropriate amount of polyethylene glycol again stir with half an hour after stirring ageing overnight with 24 hours and dried at 100^{o}C for 24 h using hot air oven. The white colour precipitate was obtained. The as prepared sample was further annealed at 500 ^{o}C for 3 h in air in order to improve the crystalline nature of the samples (sample 1). Then similar procedure was followed by synthesis of MgO nanoparticles using oxalic acid instead of PEG (sample 2). The samples with PEG and oxalic assisted MgO samples named as MP and MO, respectively.

2.3. Characterization techniques

The prepared nanopowders were successfully characterized by the following techniques. The crystalline structure and average grain size was analyzed by powder X-ray diffraction (XRD) using Bruker diffractometer within the 2θ range of 10°–80° using CuKα as X-ray source (k = 1.5406 Å). Morphology and particle size of the prepared nanoparticles was studied employing Field emission scanning electron microscope (JEOL-JSM-6390) operated at 15 kV. The elemental analysis of the samples was analyzed by EDS spectra (JEOL Model JED – 2300). The optical properties were analyzed by UV-VIS diffusion reflectance spectroscopy using CARY 5E UV-VIS-NIR spectrophotometer in the wavelength range of 200 – 900 nm. Photoluminescence spectra of the samples were recorded using PerkinElmer LS 55 spectrometer equipped with a He-Cd laser source, Excitation length used was 325 nm. XPS was analyzed by using a Thermo Scientific K-alpha surface analysis instrument.

2.4 Photocatalytic experiment set up

The photocatalytic experiment on the prepared samples for the photodegradation of dyes is performed at ambient temperature. The photocatalytic activities of MgO catalyst powders were evaluated by the degradation of phenol and CR under visible light radiation. For photocatalytic process, the dye solution was prepared by adding a particular concentration (for example 200 mL, C0 = 10 mg L-1) and a particular amount of synthesized material poured into the dye solution. In the experimental set up, 250 ml of water cooled cylindrical glass reactor with 125 W high pressure mercury lamp was used as a light source. The samples/dye solution was irradiated in the horizontal direction and the distance between the mercury lamp and the glass/dye solution was kept within 20 cm. Then the solution was kept in the dark room and well stirred with the magnetic stirrer for more than 30 min to attain the equilibrium condition throughout the solution. When the light was turned on, the experiment started. After a sudden

irradiation time, the sample was taken out from the reactor. The concentration of the aqueous suspensions (phenol and CR) in each sample was analyzed using UV–Vis spectrophotometer at a wavelength of 270 and 495 nm. The photocatalytic efficiency was calculated from the expression $\eta = (1-C/C0) \times 100$, where C0 is the concentration of dyes (phenol and CR) before illumination and C is the concentration of dyes after a certain irradiation time. The time interval of irradiation time was 20 min.

III. RESULTS AND DISCUSSIONS

3.1. Powder X-ray diffraction (XRD) analysis

The structural perfection, crystallographic nature and grain size of the sample were analyzed by using XRD method. Fig.1 shows the powder XRD pattern of MP and MO samples respectively. It can be seen that all the sharp diffraction peaks could be indexed to face center cubic structure of MgO with space group Fm-3m. The following miller indices (111), (200), (220), (311) and (222) and the calculated lattice parameter value and volume (a=4.210Å and V=74.37 $Å^3$) were matched well with the standard JCPDS data ((JCPDS file no. 89-7746).

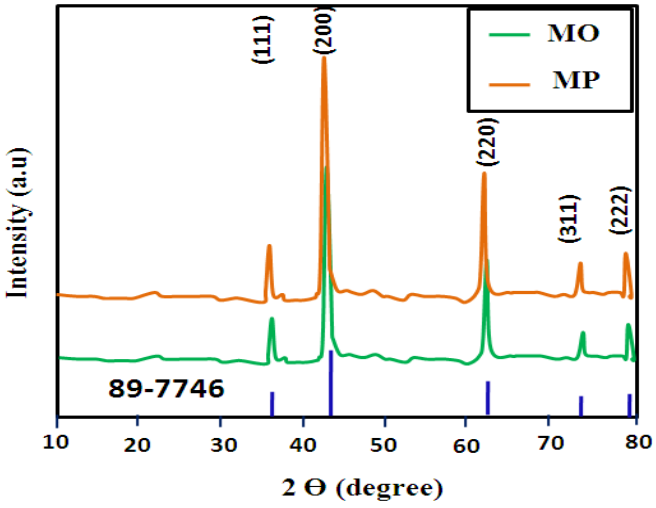

Fig. 1: Powder XRD of MgO products

It can seen that no other impurity phase were detected in the pattern, which suggest that phase purity of the MgO products. Moreover, the peak intensity of the MP sample enhanced and shifted towards the lower angle side. This result suggests that increasing the crystalline nature of MP than compared with MO. The average grain size was calculated from Full Width Half Maximum (FWHM) data using Scherrer's equation, which is given by Equation (1).

$$d = \frac{0.9\lambda}{\beta \cos\theta}$$

where d is the mean diameter of the nanoparticles, λ is the wavelength of X-ray radiation source, β is the angular FWHM of the XRD peak at the diffraction angle θ [16]. The average grain size was found to be 22 and 32 nm for MO and MP samples respectively.

3.2. FESEM and EDS analysis.

The morphology and particle size of the MgO nanostructures was examined by FESEM analysis. Fig.2 shows the FESEM images of MP and MO samples respectively. Fig. 2 a) shows the FESEM image of MP sample, it was mainly composed of nanorods with clearly individual morphology with average dimensions about 50–80 nm and length of 400-500 nm. Whereas MO sample showed that sheet like morphology of MgO with thicknesses of around at 20 nm and widths of 500-600 nm (Fig. 2b). In order know the elemental composition of the samples, EDAX measurement was carried out. Fig. 2 c) and d) shows the EDAX spectra of MP and MO samples respectively. It can be seen that the nanoparticles were composed of elemental Mg and O and it is found that the nanoparticles contain 55.6% magnesium and 44.4% oxygen. It is clear that the Mg/O atomic ratio, approximated from these data is in good agreement with that of the bulk ratio. A slightly lower oxygen atomic ratio compared to that of magnesium is probably high oxygen vacancies in the MgO nanoparticles.

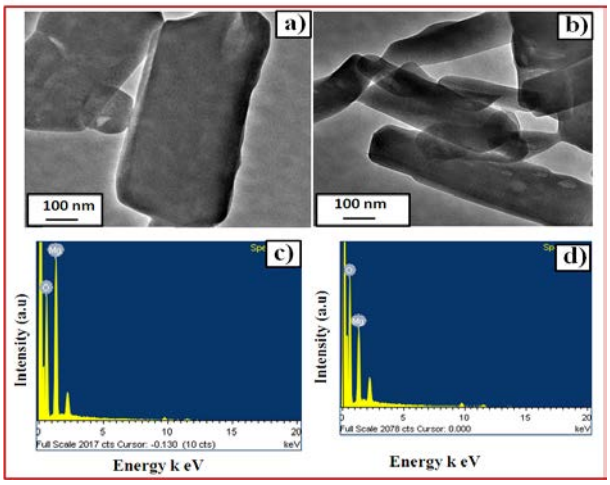

Fig. 2: (a & b) FESEM images of a) MP and b) MO; EDAX spectra of c) MP and d) MO

3.3. XPS analysis

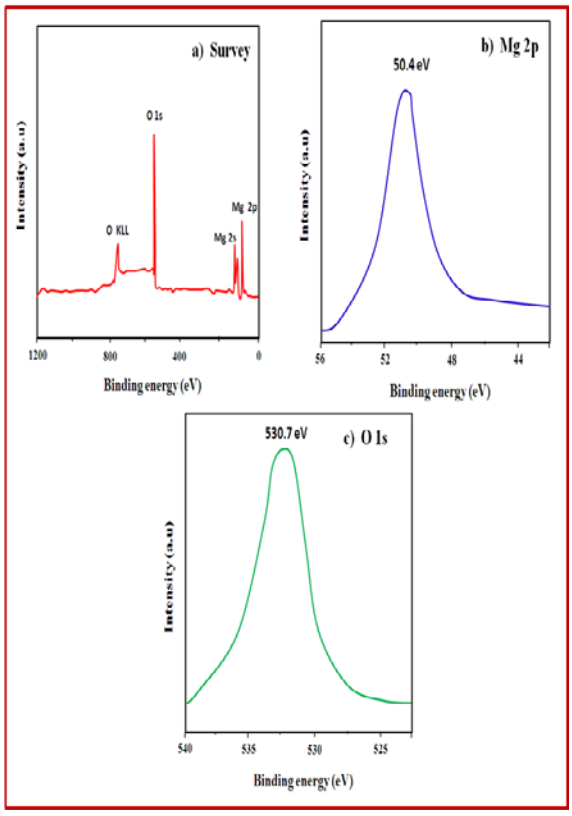

Fig. 3: XPS spectra of MgO nanoplates (MP) (a) survey spectrum (b) Mg 2p and (c) O 1s

The chemical composition and oxidation states of Mg were studied by XPS. The XPS measurements were carried out using an Mg-Ka X-ray source (hv = 1253.6 eV) with a pass energy of 50 eV. The take-off angle of X-rays in the XPS measurements is ~60^{o} relative to the sample surface. Fig. 3 shows the XPS picture of MP sample. Fig. 3 a) gives the surveyed XPS spectrum of MgO, it only consists of Mg and O lines, there are no other peaks such as C or Mo, indicating a clean MgO surface. The binding energy of Mg and O is calculated to be 50.4 and 530.7 eV respectively, which is belongs to Mg2p and O 1s band of MgO (Fig. 3 b & c). Similar findings were observed for MgO thin films [17,18]. The results suggest that Mg in 2+ oxidation state in the MgO nanocrystals.

3.4. UV-DRS analysis

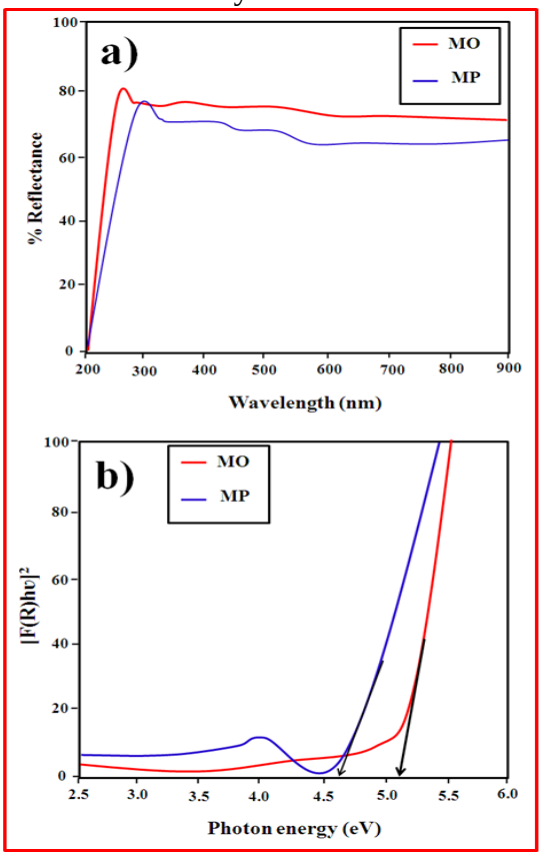

Fig.4: UV-DRS spectra of MgO (a) reflectance spectra and (b) K-M function

The optical transitions usually occur when a photon is absorbed or emitted by the defect center [19]. Therefore, optical absorption and fluorescence emission were studied to know the light absorption property and surface defect centers created on the synthesized MgO nanoparticles. Fig. 4 a) shows the UV-Vis diffuse reflectance spectra of MP and MO samples respectively. The absorption edge of MP sample was found as 240 nm, further it was shifted to higher wavelength side (~265 nm). A considerable red shift in the absorption edge was indicates that decreasing the band gap of MgO by by addition of PEG. The high wavelength of the surface exciton associated with it indicating low coordination. This is because electrostatic potential of a O_2^- ion in MgO gradually decreased as the coordination decrease, and on the whole process needs less energy. In order to further confirm the band gap (E_g), we have using Kubelka – Munk (K-M) model [19] is described below. The K-M model at any wavelength is given by F (Rα) = (1-R)^2/2R, where R is the percentage of reflectance. A graph is plotted between [F (R_α) hυ]^2 Vs hυ and the intercept

value is the direct band gap energy [20]. The optical band gap energy was found to be 5.16 and 4.67 eV for MO and MP samples respectively. Hence, we expect that that MP sample has more absorption in the visible light and would be a promising potential application in photocatalyst.

3.5. Photoluminescence analysis

Photoluminescence spectroscopy is a very important tool to explore the surface defects, impurities, energy bands, and exciton structure. Figure 5 displays the room temperature PL spectra of MgO nanoparticles with an excitation wavelength of 270 nm in the range of 200–800 nm. The PL emission spectrum exhibits three emission peaks located at 430, 468, and 490 nm in 400–500 nm emission band range, in which the 430 nm emission is due to defect band transition and 3B1u → 1Ag from F22+ defect centre occupied in D2h symmetry [21, 22]. The 465 and 495 nm blue emissions are owing to the recombination of electrons with oxygen vacancies (i.e., F centre).

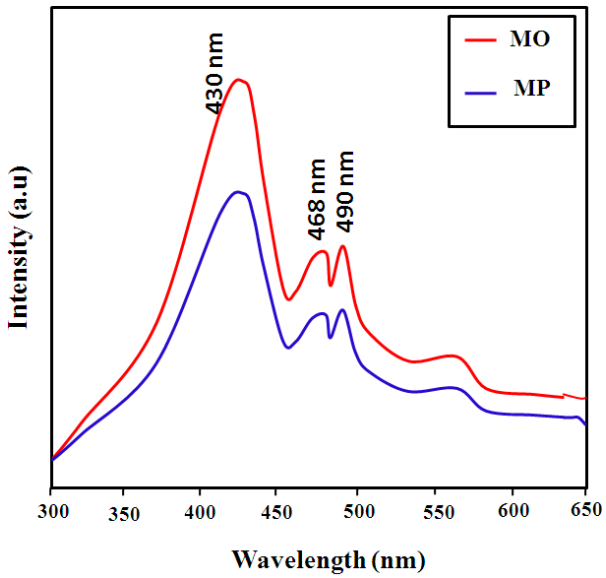

Fig.5. Room temperature PL spectra of MgO nanoproducts

These vacancies are possibly generated by various factors, namely, insufficient oxygen during annealing process, subsequential crystallization process, and Mg vacancies and interstitials [23]. It was noted that all the emission peak intensities decreases for MP sample when compared with MO sample. Generally, the peak intensity is inversely proportional to recombination of electron-hole pairs. The above result suggests that MP sample is more preferable in the photocatalytic performance.

3.6. FTIR analysis

FTIR is plausibly the utmost dominant tool for identifying the functional groups or the types of chemical bonds. Fig. 6 depicts the room temperature FTIR spectra of MgO nanoparticles. The vibration peak appeared at 3468 cm^{-1} is due to O-H stretching band. The peaks at 1440–1592 cm-1 show the bending vibration of Mg-OH stretching. Whereas, the peak at 662 cm^{-1} is due to stretching vibrations of the bond between Mg and O in MgO NPs. The presence of O-H stretching vibration is probably due to re adsorption of water molecules from the ambient atmosphere. The FTIR results again supported that formation of MgO nanocrystals.

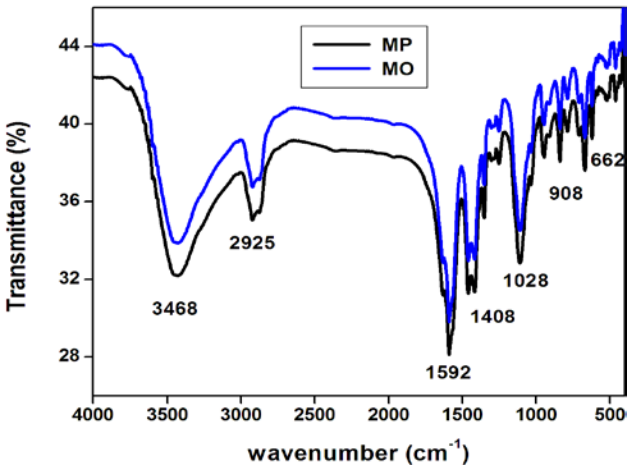

Fig.6: FTIR spectra of MgO nanoproducts

3.7. Photocatalytic test

3.7.1. UV-Vis absorption test.

In the present work, phenol and CR dyes were used as model pollutants to evaluate the photocatalytic activity of MgO nanoparticles under visible light irradiation. Both phenol and CR dyes are important class of synthetic organic dyes used in the textile industries and are common industrial pollutants. While the band gap energy of MgO is much larger than the energy of UV illumination, the generation of reactive species like •OH radicals might take place due to the native defects. Figure 7 a) & b) shows the photo-degradation characteristics of phenol dye using MP and MO samples respectively. Similarly, the time-dependent UV–Vis absorption spectrum of CR dye solutions in the presence of MP and MO samples

is depicted in Fig. 7 c) & d). As demonstrated, increasing the expose time of UV irradiation would result in a decrease of λ_{max} (phenol =270 nm; CR=495 nm) in UV-Vis spectrum. However, the decline rate of absorbance values at λ_{max} is noticeably different for both samples. In both cases, the relative absorption peak intensity was drastically decreases with the increase of visible light illumination. Hence, we conclude that both the catalyst powders were photo active materials.

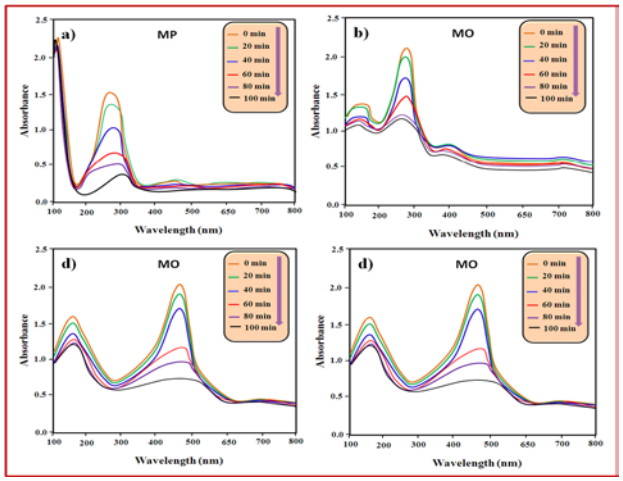

Fig. 7: Shows the UV-light absorbance of phenol (λmax = 270 nm) as a function of irradiation time (a) MP and (b) MO: absorbance spectra of CR (λmax = 495 nm) as a function of irradiation time (c) MP and (d) MO

3.7.2. Degradation efficiency.

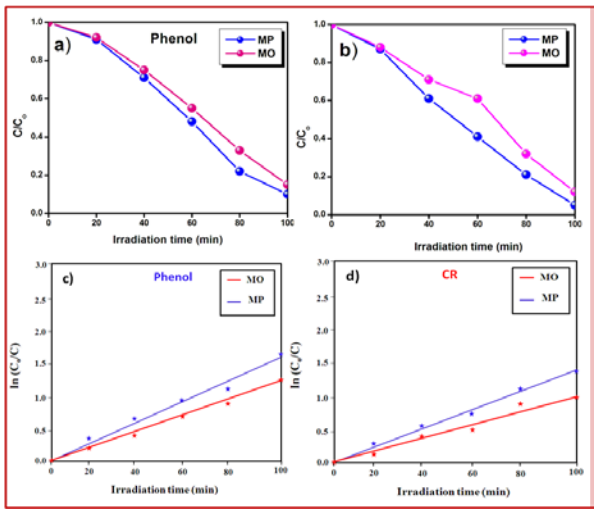

Fig. 8: (a) shows the temporal degradation profile of phenol and (b) degradation profile of CR (c) kinetic fit for the degradation of phenol (d) kinetic fit for the degradation of CR under visible light irradiation.

The samples were further tested for degradation efficiency test. Fig. 8 a) & b) shows the temporal degradation profile for phenol and CR dyes using MgO catalyst powders under visible light irradiation. The degradation efficiency of phenol was found to be 90 and 85% for MP and MO samples respectively. Similarly, the degradation efficiency of CR was found to be 95 and 88% for MP and MO samples respectively. The results suggest that MP sample showed superior photocatalytic efficiency towards phenol and CR dyes than that of MO sample. This could be due to could be due to the number of dye molecules (phenol and CR) that can interact with the active surfaces of MgO nanoplates are large compared to of MgO nanorods. In addition, smaller band gap energy and oxygen deficient MgO nanosheets also another crucial role to enhancing the catalytic performance.

3.7.3. First order kinetic studies

In order to get the accurate kinetic data, the rate constants of photodecomposition of phenol and CR dyes were calculated according to the following first-order kinetics [24]:

$$\ln C/Co = -kt,$$

where C0 is the initial concentration of the dyes, C is the concentration of the dyes, k is a rate constant and t is the reaction time. Figs. 8 (c & d) show the kinetic fit for the degradation of phenol and CR under visible light irradiation. After a simple calculation, k value of phenol is found as 0.3432 and 0.2573 min-1. Similarly, the CR is 0.4424 and 0.3259 min-1 for MP and MO samples, respectively. Table 1 summarizes the other photocatalytic parameters of these samples.

3.7.4. Recycle test

In view of the practical applications for photocatalysts, the reusability and stability of the MgO nanostructures are of significance. Fig. 9 (a-d) shows the recycling test of MgO catalyst powders under UV light irradiation. It can be seen that after 7 cycle, only small variation was observed in the photocatalytic efficiency. The slight variation in the photocatalytic degradation is due to the incomplete collection of the samples by the centrifugation process. These results suggest that MgO catalyst showed good stability and recyclability. Hence, this type of catalyst powders might be a promising potential application in high performance photocatalytic device.

3.7.5. Photocatalytic mechanism

When the visible light irradiate on the MgO surface, MgO may absorb visible light and capture the photo-induced electron into the MgO conduction band, which can generate the formation of very reactive radicals, hydroxyl radical OH- and superoxide radical ion O2-, both radicals are crucial role for the degradation of the dye solutions. In our case, MP sample (nanoplates) showed high photocatalytic performance. This could be due to large active sites (plate like) facilitate the reaction/interaction between the photocatalyst and the dye molecules.

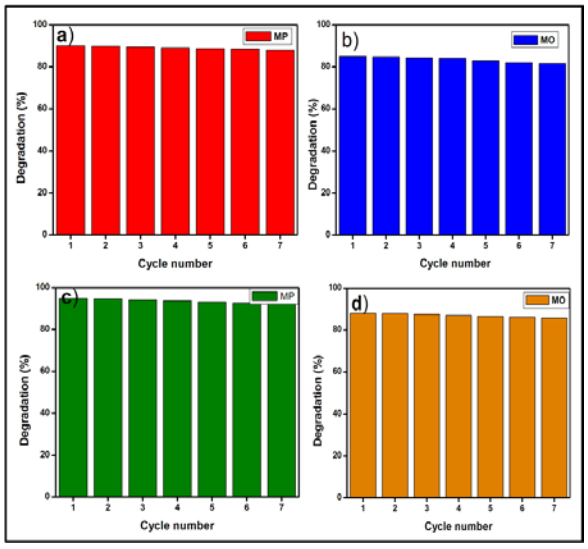

Fig. 9: Recycling test of phenol (a) MP and (b) MO (seven cycle segment) and recycling test of CR (c) MP and (d) MO

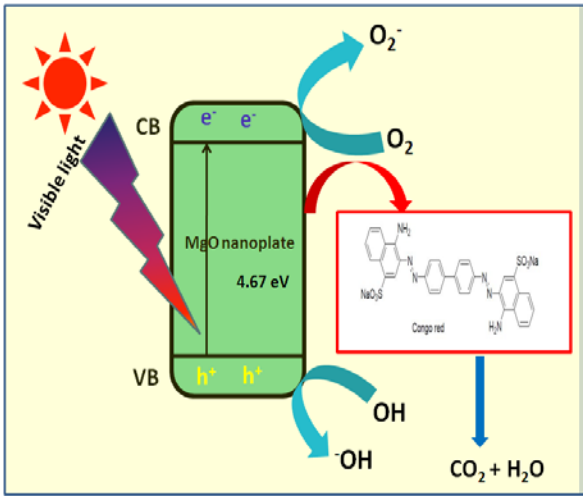

Fig.10. Photocatalytic mechanism of MgO under visible light irradiation.

These chemically more active atoms play a major role in enhancing the photocatalytic reaction. Besides, with the decrease in the band gap of MP sample, which results in the recombination rate of electrons and holes will be reduced, and more electrons and holes that are generated will be transferred to the surface of the catalysts and subsequently enhances the catalysis. As clear from the PL spectra the presence of an expansive number of defect sites can likewise make the catalysts with high chemical activities. The photogenerated electrons and holes in these defects levels also act as the active sites for the photocatalytic response since they can also be trapped by the oxygen and surface hydroxyl species. Therefore, the experimental results demonstrate that MgO nanoparticles possess excellent photocatalytic activity for phenol and CR dyes under visible light illumination.

Table. 1: Comparison of band gap energy, rate constant and photocatalytic degradation efficiency of MgO nanoproducts

Samples	Band gap (eV)	Rate constant of MB		Rate constant of CR		Degradation efficiency at 100 min	
		K (min^{-1})	R^2	K (h^{-1})	R^2	MB	CR
MP	5.16	0.3432	0.923	0.4424	0.912	90	85
MO	4.67	0.2573	0.947	0.3259	0.958	95	88

IV. CONCLUSION

We have successfully prepared MgO nanocrsystalline with nanoplatelets and nanorods shaped morphology via a facile sol gel method. Powder X-ray diffraction analysis showed that the nanostructures consisted of cubic-phase MgO. When PEG and oxalic acid and were added to the reaction system. A considerable red shift in the absorption edge and decreasing the band gap was observed for nanosheets of MgO. XPS analysis confirms that Mg in 2+ state in MgO nanocrystals. The photocatalytic activity of phenol and CR was enhancing by MgO nanosheets when compared to MgO nanorods. This could be due to could be due to the number of dye molecules (phenol and CR) that can interact with the active surfaces of MgO nanosheets are large compared to of MgO nanorods. This method can be easily scaled up to produce high surface area with desired morphology and is expected to be a promising

industrial production process of MgO for different catalytic and separation processes.

REFERENCES

[1] S. Girish Kumar, L. Gomathi Devi, "Review on modified TiO_2 photocatalysis under UV/visible light: selected results and related mechanisms on interfacial charge carrier transfer dynamics," Journal of Physical Chemistry A; vol. 115**,** pp. 13211-13241, 2011.

[2] J. Schneider, M. Matsuoka, M. Takeuchi, J. Zhang, Y. Horiuchi, M. Anpo, D. W. Bahnemann, "Understanding TiO_2 photocatalysis: mechanisms and materials" Chemical Reviews; vol. 114, pp. 9919-9986, 2014.

[3] L. Liu, X. Chen, "Titanium Dioxide Nanomaterials: Self-Structural Modifications," Chemical Reviews; vol. 114, pp. 9890-9918, 2014.

[4] S. W. Vergruggen, "TiO_2 photocatalysis for the degradation of pollutants in gas phase: From morphological design to plasmonic enhancement," Journal of Photochemistry and Photobiology C: Photochemical Reviews. vol. 24, pp. 64-82, 2015.

[5] G.R. Duan, X.J. Yang, J. Chen, G.H. Huang, L.D. Lu, X. Wang, "Nitrated graphene oxide and its catalytic activity in thermal decomposition of ammonium perchlorate," Powder Technol; vol. 172, pp. 27-29, 2007.

[6] K. He, Y.M. Dong, Z. Li, L. Yin, A.M. Zhang, Y.C. Zheng, "Catalytic ozonation of phenol in water with natural brucite and magnesia," J. Hazard. Mater; vol.. 159, pp. 587–592 2008.

[7] T. Selvamani, T. Yagyu, S. Kawasaki, I. Mukhopadhyay, "Easy and effective synthesis of micrometer-sized rectangular MgO sheets with very high catalytic activity, Catal. Commun. Vol 11, pp. 537–541, 2010.

[8] S.A. El-Molla, S.M. Abdel-all, M.M. Ibrahim, Influence of Precursor of MgO and preparation conditions on the catalytic dehydrogenation of iso-propanol over CuO/MgO catalystsJ," Alloys Compd; vol. 484, pp.280–285, 2009.

[9] A. Tompos, J.L. Margitfalvi, E.G. Szabó, Z. Pászti, I. Sajó, G. Radnóczi, Role of modifiers in multi-component MgO-supported Au catalysts designed for preferential CO oxidation, J. Catal; vol. 266, pp. 207–217, 2009.

[10] D. Gulkova´ , O. Solcova´ , M. Zdrazil, Preparation of MgO catalytic support in shaped mesoporous high surface area form, Microporous Mesoporous Mater; vol. 76, pp. 137–149, 2004.

[11] Y.H. Wang, H.M. Liu, B.Q. Xu, J. Mol. Durable Ni/MgO catalysts for CO2 reforming of methane: Activity and metal-support interaction, Catal. A: Chem. Vol. 299, pp. 44–52, 2009.

[12] J. Reis, R. Chaim, Densification maps for spark plasma sintering of nanocrystalline MgO ceramics: Particle coarsening and grain growth effects, Mater. Sci. Eng; A vol. 491, pp. 356–363, 2008.

[13] D.Y. Chen, E.H. Jordan, M. Gell, Pressureless sintering of transclucent MgO ceramaics, Scripta Mater; vol. 59, pp. 757–759, 2008.

[14] R. Sathyamoorthy, K. Mageshwari, S.S. Mali, S. Priyadharshini, P.S. Patil, Effect of organic capping agent on the photocatalytic activity of MgO nanoflakes obtained by thermal decomposition route, Ceram. Int; vol. 39, pp. 323–330, 2013

[15] N. Sutradhar, A. Sinhamahapatra, S.K. Pahari, P. Pal, H.C. Bajaj, I. Mukhopadhyay, A.B. Panda, J. Phys. Chem. C; vol. 115,pp. 12308–12316, 2011.

[16] M. Parthibavarman, K. Vallalperuman, S. Sathishkumar, M. Durairaj M. Thavamani, A novel microwave synthesis of nanocrystalline SnO2 and its structural, optical and dielectric properties J. Mater. Sci.: Mater. Electron; vol. 25, pp. 730-735, 2014.

[17] S. A. Chambers, Epitaxial growth and properties of thin film oxides, Surf. Sci. Rep. vol. 39, pp. 105- 180, 2000.

[18] V. E. Henrich and P. A. Cox, The Surface Science of Metal Oxides, Academic, Cambridge, 1994.

[19] M. Karthik, M. Parthibavarman, A. Kumaresan, G. Prabhakaran, V. Hariharan, R. Poonguzhali, S. Sathishkumar, One-step microwave synthesis of pure and Mn doped WO_3 nanoparticles and its structural, optical and electrochemical properties.Journal of Materials Science: Materials in Electronics; vol. 28, pp. 6635-6642, 2017.

[20] V. Hariharan, S. Radhakrishnan, M. Parthibavarman, R Dhilipkumar, C. Sekar, Synthesis of polyethylene glycol (PEG) assisted tungsten oxide (WO3) nanoparticles for l-dopa bio-sensing applications. Talanta; vol. 85, pp. 2166 – 2174, 2011

[21] N. C. S. Selvam, R. T. Kumar, L. J. Kennedy, and J. J. Vijaya, Comparative study of microwave and conventional methods for the preparation and optical properties of novel MgO-micro and nano-structures, J. Alloy. Compd; vol. 509, pp. 9809–9815, 2011.

[22] A. Kumar, S.Thota, S. Varma, and J. Kumar, Sol-gel synthesis of highly luminescent magnesium oxide nanocrystallites, Journal of Luminescence; vol. 131, pp. 640–648, 2011.

[23] Y. Hao, G. Meng, C. Ye, X. Zhang, and L. Zhang, Kinetics driven growth of orthogonally branched single-crystalline magnesium oxide nanostructures, Journal of Physical Chemistry B; vol. 109, pp. 11204–11208, 2005.

[24] M. Farhadian, P. Sangpour, G. Hosseinzadeh, Preparation and photocatalytic activity of WO3-MWCNT nanocomposite for degradation of naphthalene under visible light irradiation. RSC Adv; vol. 00, pp. 1-11, 2016.